JOURNAL OF GEOPHYSICAL RESEARCH, VOL. 112, D02209, doi:10.1029/2006JD007500, 2007

Measurements of heterogeneous ice nuclei in the western United States in springtime and their relation to aerosol characteristics

Mathews S. Richardson,[1] Paul J. DeMott,[1] Sonia M. Kreidenweis,[1] Daniel J. Cziczo,[2,3] Edward J. Dunlea,[4] Jose L. Jimenez,[4] David S. Thomson,[5] Lowell L. Ashbaugh,[6] Randolph D. Borys,[7] Douglas L. Westphal,[8] Gary S. Casuccio,[9] and Traci L. Lersch[9]

Received 11 May 2006; revised 8 September 2006; accepted 29 September 2006; published 31 January 2007.

[1] The second Ice Nuclei Spectroscopy (INSPECT-II) campaign was conducted at Storm Peak Laboratory in northwestern Colorado in April and May 2004. The physical and chemical characteristics of springtime atmospheric aerosols, including those which act as heterogeneous ice nuclei (IN), were investigated. The ice formation activity of submicron particles was measured with a continuous-flow diffusion chamber. The concentrations of heterogeneous ice nuclei ([IN]) active at -15 to -50°C and water supersaturations $-25\% < SSw < 0$ typically ranged from 1 to 10 std l^{-1}. Aerosol mass spectrometry measurements indicated that the composition of IN had much higher contributions from mineral dust/fly ash and metallic particle types compared to ambient particles of similar sizes. While IN concentration and composition measurements are similar to observations from the same site during INSPECT-I in November 2001, there was considerably more variability in [IN] during INSPECT-II associated with periods of sporadically high [IN]. A relation of [IN] to concentrations of larger particles was noted; however, the predictive utility of such a relationship proved limited during non-dust-related increases in accumulation mode number concentrations. We conclude that the observed high variability and extremes in [IN] during spring are attributable primarily to variations in airborne dust concentrations and that the [IN] observed in spring 2004 represent lower bounds on the expected [IN] at SPL in the spring. On the basis of modeled dust vertical profiles, strong impacts of dust on [IN] might be expected at the higher altitudes of cold clouds.

Citation: Richardson, M. S., et al. (2007), Measurements of heterogeneous ice nuclei in the western United States in springtime and their relation to aerosol characteristics, *J. Geophys. Res.*, *112*, D02209, doi:10.1029/2006JD007500.

1. Introduction

[2] Ice nucleation in clouds can proceed by two different pathways: heterogeneous or homogeneous nucleation. Significant homogeneous nucleation proceeds at temperatures below about -38°C near water saturation and at progressively lower relative humidities at lower temperatures. On the other hand, heterogeneous ice nucleation can proceed at relative humidities closer to ice saturation as well as at temperatures significantly above -38°C. Heterogeneous nucleation typically requires an insoluble substrate, termed an ice nucleus (IN). Because these IN activate at temperatures above or saturations below those required by homogeneous nucleation, even in relatively small concentrations, IN have the ability to significantly alter cold cloud properties. The impact of IN on cold cloud properties and formation is complex and is also dependent on large and small-scale dynamics [*Gierens*, 2003; *Haag and Kärcher*, 2004; *Kärcher*, 2004]. Recent studies have postulated that ice nuclei have the potential to alter the radiative properties of cirrus, play a role in the dehydration of the tropical tropopause layer [*Kärcher*, 2004], affect convective cloud dynamics [*Liu et al.*, 1997; *van den Heever and Cotton*, 2004] and enhance or inhibit convective precipitation [*Gilmore et al.*, 2004]. *Haag and Kärcher* [2004] propose that increases in the abundance of IN in the mid to upper troposphere can result in increased occurrence of cirrus clouds. The paucity of data on atmospheric IN concentrations ([IN]) hampers the evaluation of these hypotheses. Similarly, data on IN com-

[1]Department of Atmospheric Science, Colorado State University, Fort Collins, Colorado, USA.
[2]Aeronomy Laboratory, NOAA, Boulder, Colorado, USA.
[3]Now at Institute for Atmospheric and Climate Science, Swiss Federal Institute of Technology, Zurich, Switzerland.
[4]Department of Chemistry and Biochemistry, Cooperative Institute for Research in Environmental Science, University of Colorado, Boulder, Colorado, USA.
[5]Earth System Research Laboratory, NOAA, Boulder, Colorado, USA.
[6]Crocker Nuclear Laboratory, University of California, Davis, California, USA.
[7]Storm Peak Laboratory, Division of Atmospheric Science, Desert Research Institute, Reno, Nevada, USA.
[8]Naval Research Laboratory, Monterey, California, USA.
[9]RJ Lee Group, Inc., Monroeville, Pennsylvania, USA.

0148-0227/07/2006JD007500$09.00

position, their potential sources and their magnitudes are sparse.

[3] One type of particle long known to be effective in catalyzing ice formation is mineral dust [*Roberts and Hallett*, 1968]. Many prior lab studies have shown that certain minerals nucleate ice formation at temperatures well above −38°C [*Pruppacher and Klett*, 1997], and recent work [*Archuleta et al.*, 2005; *Zuberi et al.*, 2002] demonstrated that mineral particles coated in sulfate can cause freezing of sulfate solutions at temperatures up to 10° warmer than required for pure sulfate droplets. Recent field observations have provided strong evidence for a link between naturally occurring dusts and formation of ice in clouds. For example, Asian dust plumes have been associated with warmer-than-average cirrus cloud top temperatures and lower cloud bases over the western United States [*Sassen*, 2002]. *Sassen* [2005] also observed occurrence of ice-crystal clouds at relatively warm temperatures and ice saturations just greater than unity over Alaska, and found these events were associated with elevated dust layers attributable to Asian dust storms. Researchers observed incursions of Saharan dust plumes in the midtroposphere over Florida during the Cirrus Regional Study of Tropical Anvils and Cirrus Layers–Florida Area Cirrus Experiment (CRYSTAL-FACE) in summer 2002. These plumes were associated with elevated concentrations of ice nuclei [*DeMott et al.*, 2003b] and glaciation of modestly supercooled clouds [*Sassen et al.*, 2003]. Finally, several studies that examined the composition of atmospheric particles detected as IN or present in cloud crystal residuals have shown that mineral particles are frequently a dominant particle type [*Chen et al.*, 1998; *Cziczo et al.*, 2004; *DeMott et al.*, 2003a; *Heintzenberg et al.*, 1996; *Twohy and Poellot*, 2005].

[4] Arid regions of the southwestern United States are sources of dust to the mid and upper troposphere over the U.S. West [*Prospero et al.*, 2002]. However, prior studies have shown that during spring, storms over arid and semiarid regions in Asia loft large masses of dust to the middle troposphere [*Takemi*, 2005]. Dust concentrations in these plumes are often large enough to be detected as far east as the Midwestern United States [*Augustine et al.*, 2003; *Husar et al.*, 2001]. In a climatological study of Asian dust events over the United States, *VanCuren and Cahill* [2002] found that Asian dust and its accompanying pollutants are transported year-round to the United States, and the maximum in intensity for the western United States occurs in late spring.

[5] The need for additional data on free-tropospheric IN abundance and composition was the motivation for the Ice Nuclei and Spectroscopy campaign (INSPECT-I) that took place in November 2001 at the Desert Research Institute's Storm Peak Laboratory (SPL) in Northwest Colorado. The lab's elevation (3210 meters above mean sea level, MSL) allows sampling of free tropospheric air for extended periods of time [*Borys and Wetzel*, 1997]. In general, [IN] measured during the campaign were quite low. Particle types identified as active IN included those containing metallics, although the most prevalent types were representative of naturally derived mineral particles [*DeMott et al.*, 2003a]. The results and the possibility that both Asian and U.S. dust sources may contribute to dust-derived IN over the western United States motivated a return to the SPL site for an expanded study (INSPECT-II) during April and May 2004, timed to coincide with the period of peak Asian dust transport to the western United States. This paper reports results from the INSPECT-II campaign and compares IN characteristics with those observed in INSPECT-I and other earlier studies.

2. Methodology

[6] The location of SPL (106.73°W by 40.45°N) is shown in Figure 1. For this study, a suite of instruments collected data intended to characterize the physical and chemical properties of the ambient aerosol. The Colorado State University Continuous Flow Diffusion Chamber (CFDC [*Rogers*, 1988]) measured the concentrations of ice nucleating particles as functions of the aerosol temperature and ice saturation ratio. A quadrupole Aerodyne Aerosol Mass Spectrometer (Q-AMS [*Jayne et al.*, 2000; *Jimenez et al.*, 2003]) obtained speciated and size-resolved aerosol mass concentrations for nonrefractory species from 40 nm to 1.0 micron. NOAA's Particle Analysis by Laser Mass Spectrometry (PALMS [*Thomson et al.*, 2000]) measured single-particle size and composition for particles ranging in size from 200 nm to 3 microns with the transmission efficiency dropping significantly beyond 1 micron. Daily, 24-hour-integrated aerosol filter samples were obtained using samplers and protocols identical with those employed in the IMPROVE (Interagency Monitoring of Protected Visual Environments) network. Filters were analyzed for composition and aerosol mass concentrations of particulate matter with aerodynamic diameters smaller than 2.5 micron ($PM_{2.5}$) and smaller than 10 microns (PM_{10}). Ambient temperature, pressure, relative humidity, and other standard meteorological measurements were obtained from the laboratory's weather station.

[7] The sampling configuration used for the CFDC, AMS and PALMS during the campaign is shown in Figure 2. A cyclone with a 50% cut point of 1 micron continuously sampled from the free airstream at an elevation of 10 m above the laboratory roofline. Flow through the inlet was divided into three sample streams: one sent to the AMS or PALMS, one to the CFDC, and the third controlled as makeup flow to maintain the total flow required for the cyclone cut point. A Perma Pure, MD-series gas drier (Perma Pure, LLC; Toms River, NJ) dried the CFDC sample stream with a 2:1 sheath-to-sample counterflow of dry nitrogen. Downstream of the CFDC, a Pumped Counter Flow Virtual Impactor (PCVI) selected ice crystals larger than 1.5 μm for additional analyses [*Boulter et al.*, 2006].

[8] In addition to the above measurements, several other concentration and size measurements supported the analysis of the composition and IN concentration data as in the work by *Lowenthal et al.* [2002]. An Ultrafine Particle Counter (TSI 3025A; TSI Inc., Shoreview, MN) and Condensation Particle Counter (TSI 3010) measured total particle concentrations down to ~3 nm. A Scanning Mobility Particle Sizer (SMPS; TSI 3936) measured fine particle size distributions while an Aerodynamic Particle Sizer (APS; TSI 3321) measured the coarse mode distribution. A LASAIR optical particle counter (OPC; PMS 1002; Particle Measuring Systems, Boulder, CO) measured the accumulation mode

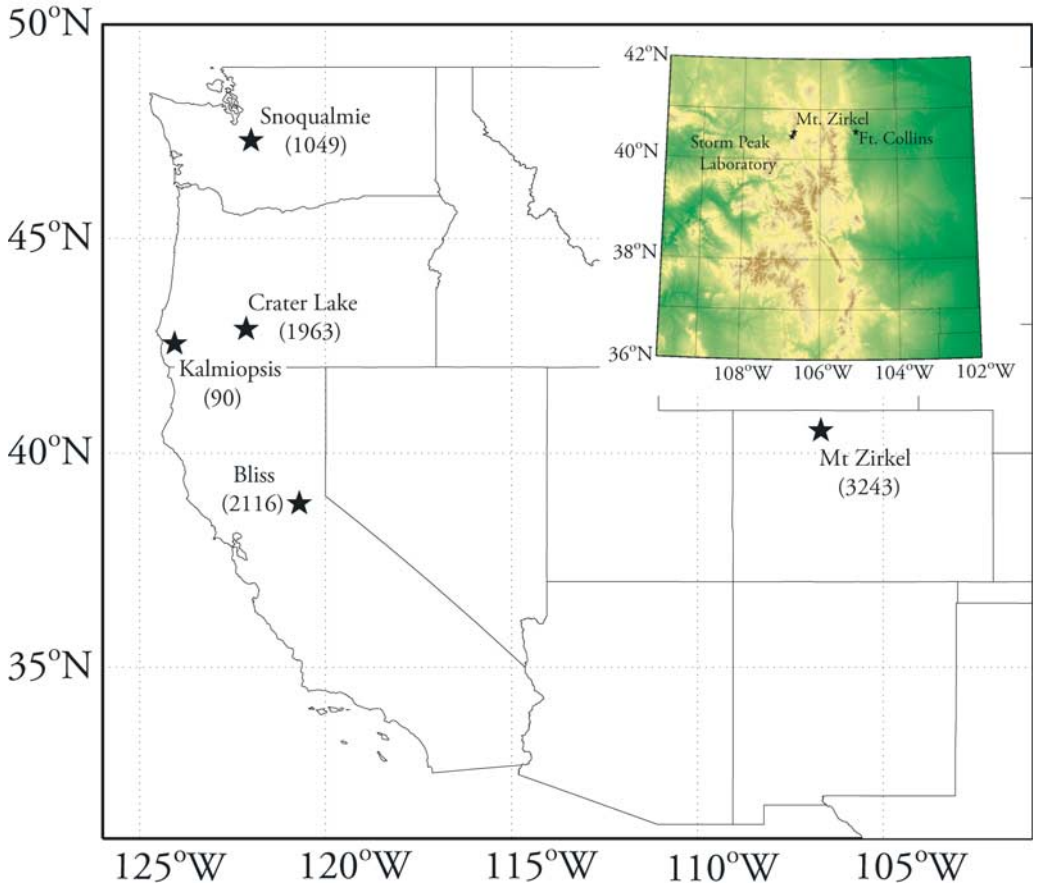

Figure 1. Location of IMPROVE sites referenced in this study. Numbers in parentheses show the elevation of the sampling site in meters. Inset shows the topography of Colorado and the locations of Storm Peak Laboratory (SPL), the Mt. Zirkel IMPROVE site, and Fort Collins in the Front Range.

distribution (optical diameters greater than 0.1 μm). A Dasibi ozone monitor (Dasibi Environmental Corp.; Glendale, CA) collected ozone concentrations. CO was measured by a Thermo Environmental Instruments Model 48S (TEI; Franklin, MA) modified according to *Parrish et al.* [1994]. A Thermo Environmental Instruments Model 43 S (TEI; Franklin, MA) measured sulfur dioxide concentrations.

2.1. Continuous Flow Diffusion Chamber

[9] The CFDC consists of two concentric, ice-coated cylinders held at different temperatures. In this study, the inner wall temperature was lower than the outer wall temperature thereby setting up a linear temperature and water partial pressure gradients in the annular gap resulting in a region of supersaturation with respect to ice [*Rogers*, 1988]. Since the walls are coated with ice, vapor pressure in the annular gap is calculated assuming ice saturation at the respective wall temperatures using formulas for ice saturation vapor pressure described by *Buck* [1981]. A particle free sheath flow consisting of dry, high purity (99.998%) nitrogen (Scott Specialty Gas; Plumsteadville, PA) confined the sample flow entering the chamber to a thin lamina near the center of the annular region.

[10] A laminar flow element (LFE) maintained at laboratory temperatures measured the sample flow rate ($\sim$1 to 2 lpm). The LFE was located immediately downstream of a 404 micron orifice (O'Keefe Controls; Trumbull, CT) and upstream of the CFDC (Figure 2). The orifice maintained a chamber pressure of 450 to 500 mbar for the operation of the PCVI (located downstream of the CFDC, Figure 2). This lower pressure also created higher crystal mass growth rates attributable to increased water vapor diffusivity [*Pruppacher and Klett*, 1997]. A volumetric flow controller (VC-20LPM; Alicat Scientific, Tucson, AZ) maintained a sheath flow rate of 9 lpm for the campaign.

[11] On the basis of the total flow rate, particle residence times in the growth region ranged from approximately 3 to 4 s. The refrigeration system consisted of two separate vapor compression systems. For the colder temperatures of the inner wall, a two-stage vapor compression system cooled the inner wall. The core of the inner wall contained a heat transfer fluid, Syltherm (The Dow Chemical Company;

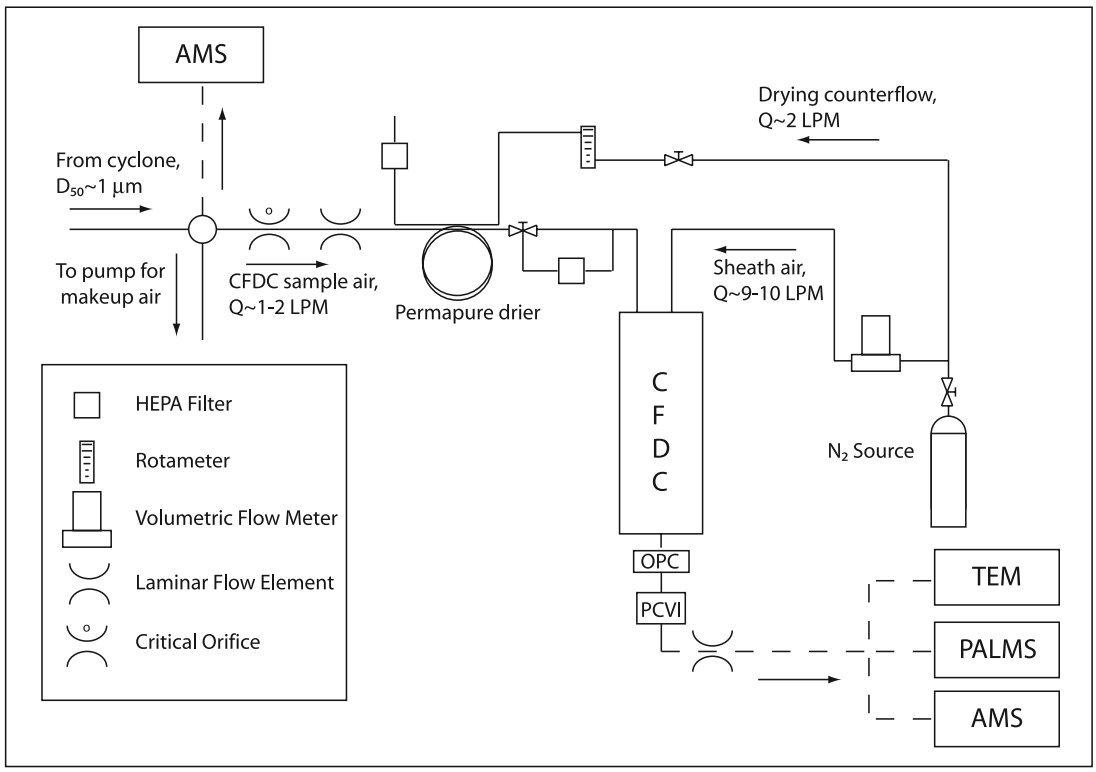

Figure 2. Experimental setup used for aerosol sampling at Storm Peak Laboratory during INSPECT-II. The dashed lines indicate flow to instruments that were alternately in place for sampling downstream of the CFDC. In addition to measurements shown here, ambient aerosol was sampled on TEM grids and by the PALMS and AMS during periods when the CFDC was not operational.

Midland, MI), to minimize temperature gradients along the cold wall.

[12] The length of the chamber is 81 cm; the final 30 cm of the warm cylinder is not coated with ice to create a water subsaturated environment for the evaporation of any activated but unfrozen cloud droplets. This evaporative region prevents the false detection of these drops as ice crystals. An OPC (Climet Instruments Company; Redlands, CA) detected particles immediately downstream of the CFDC. Particles with optical diameters larger than 2 μm are classified as ice crystals, and their number concentrations are reported as [IN]. The data acquisition system acquired counts at 1 Hz. Discrete, 1-min averages of these acquired counts are reported below.

[13] The CFDC processed particles over a range of conditions throughout the campaign, from -15°C to -50°C and to water saturation ratios as high as 1.21. A single experiment at temperatures below -35°C generally covered ice saturation ratios required for both homogeneous and heterogeneous nucleation. Data presented in the following sections are exclusively a result of heterogeneous nucleation. Data at temperatures below -35°C indicate nucleation by deposition or freezing nucleation and represent only those particles active as IN at relative humidity below values required for the onset of homogeneous freezing nucleation of solution droplets.

[14] The CFDC sample stream was periodically diverted through a filter (Figure 2) to measure background counts attributable to ice shed from the walls and to electronic noise. A 15 s lag after the sample stream was switched was excluded from the 1 min average to allow the chamber to be completely flushed. During postprocessing, the 1 min filter data were examined for significant trends. Trends in the data from the filtered air sample were fit with the appropriate curve (or curves, if necessary) as a function of time using the Matlab Curve Fitting Toolbox (The MathWorks, Natick, MA). Prediction bounds were calculated for new observations at a confidence level of 95% [*Crow et al.*, 1960] from these fits. The upper prediction bound was then subtracted from the 1 min sample concentrations to generate corrected [IN].

[15] Sparse and aperiodic extreme frost events occur within the chamber resulting in anomalously high [IN]. These events occur when vapor deposited on the cold wall forms frost crystals large enough to produce splinters that break off and become entrained in the mean flow [*Rogers*, 1994]. During IN measurements under conditions supporting only heterogeneous nucleation, 1 Hz OPC counts are dominated by counts of 0 and 1. Frost events are acute and generate 1 Hz OPC counts exceeding approximately 3 (roughly equivalent to $\sim$120 IN per liter). To prevent overestimation of IN concentrations, the 1 min data set was further corrected by setting these high 1 Hz events to 0 and reaveraging the periods in which these events occurred.

[16] As described by *Rogers* [1988], CFDC sample processing conditions (i.e., water saturation ratio and temperature) are calculated on the basis of the average wall temperatures computed from temperatures returned from an

array of thermocouples located along each wall [*Rogers et al.*, 2001]. During INSPECT-II, a particularly strong (3° to 4.5°C) axial temperature gradient existed along the cold wall. For this reason, sample conditions based on computed average temperatures were not representative of the actual aerosol processing conditions. A series of laboratory studies provided data for post processing reanalysis to determine the actual sampling conditions. These experiments determined the "effective" cold wall temperature required for the onset of homogeneous freezing of ammonium sulfate solution drops with an initial dry diameter of 100 nm. This analysis used results from previous laboratory studies [*Chen et al.*, 2000] and yielded a simple linear relationship between the measured and "effective" cold wall temperature. All data reported here have been corrected using this approach. Data reported here are corrected to standard temperature and pressure (STP; P_0 = 1013.25 mbar and T_0 = 0°C), but are not corrected for particle losses within the sampling system.

2.2. Measurements of Particle Composition

2.2.1. PALMS

[17] PALMS measures the composition of single particles using laser desorption and ionization (LDI) [*Thomson et al.*, 2000]. In this campaign, PALMS alternately measured the ambient aerosol chemical composition and the composition of ice crystal residuals downstream of the CFDC in a configuration similar to that used in INSPECT-I [*Cziczo et al.*, 2003; *DeMott et al.*, 2003a]. In this second configuration, the PCVI separated larger particles from the sample stream exiting the CFDC, ensuring PALMS sampled only ice crystals. To prevent crystal evaporation between CFDC and PALMS, dry ice cooled the PCVI. Upon entering the PALMS instrument, an aerodynamic lens focused the sampled particles and increased their transmission efficiency [*Cziczo et al.*, 2003]. This was necessary because of the low concentrations of particles that serve as heterogeneous IN [*DeMott et al.*, 2003a, 2003b]. For particles in the range of 0.3 to 1.0 μm diameter the transmission efficiency is 10% ± 1% [*Cziczo et al.*, 2003]. Particles pass through a YAG laser beam (532 nm) in order to be detected and to trigger an excimer desorption and ionization laser (193 nm). A second YAG beam is situated at a fixed distance upstream of the detection laser to determine particle velocity, and thus size. Particles need not pass through this timing beam to be detected and analyzed, but a size is typically determined for 90% of detected particles. A time of flight mass spectrometer obtains a complete positive or negative spectrum of the particle which is then classified using a hierarchical clustering algorithm described by *Murphy et al.* [2003]. Laser ablation mass spectrometry is capable of universal detection of components but is not inherently quantitative since the ablation and ionization stage is highly dependent on particle size, shape, and composition [*Johnston*, 2000].

2.2.2. AMS

[18] Unlike PALMS, which measures the composition of single particles, the AMS instrument employed in INSPECT-II determined the composition of an ensemble of particles. The AMS consists of three sections: a sampling inlet, a particle time-of-flight (PToF) chamber and a particle composition detection chamber [*Jayne et al.*, 2000]. Each chamber is separated by an aperture and is differentially pumped. The inlet consists of an aerodynamic lens that focuses the particles into a narrow beam (<1 mm in diameter), resulting in a transmission efficiency to the detector of greater than 95% for particles with diameters between 70 and 500 nm and substantial transmission of particles with aerodynamic diameters between 40 nm and 1μm [see *Jayne et al.*, 2000, Figure 9]. Upon exiting the inlet region, particles are accelerated to a size-dependent velocity. Time-resolved particle detection at the outlet of the PToF chamber allows the determination of particle velocity and therefore aerodynamic diameter. Upon entering the detection chamber, the particle beam impacts a heated surface (~600°C) where the nonrefractory components in and on particles flash vaporize on impact. Electron impact ionizes the resulting plume and a quadrupole mass spectrometer determines the composition of the resulting ions. This results in less fragmentation than occurs with the ionization scheme used in PALMS but does not allow the detection of refractory aerosol components [*Allan et al.*, 2003]. Data are reported as size-dependent mass concentrations of component classes.

2.2.3. IMPROVE

[19] An IMPROVE sampler operated in an enclosure on the roof of the laboratory. The sampler at SPL collected particulate matter for 24 hour periods starting at 0800 local time (the typical IMPROVE protocol requires sampler operation from midnight to midnight every third day). The sampler consists of four sampling modules: three that sample fine particles (particles with aerodynamic diameter less than 2.5 μm, $PM_{2.5}$) and one that samples PM_{10}. Each sampling module has an independent inlet, critical orifice for flow control, and pump. The $PM_{2.5}$ modules use a cyclone to remove particles greater than 2.5 μm. The PM_{10} module uses a Sierra-Anderson inlet to remove particles larger than 10 μm. The three different fine mass sample modules correspond to three different filter types: Teflon, nylon and quartz. The PM_{10} sample module collected aerosol on Teflon filters. Each sample module contained four separate filters that were changed automatically over a period of 3 or 4 days. One field blank filter was collected from the sample module each week on which no air was sampled. This field blank was analyzed and the data used to correct for sampling artifacts on the nylon and quartz filters (http://vista.cira.colostate.edu/improve/Publications/SOPs/ucdavis_sops/sop351.pdf).

[20] The Teflon filters were analyzed gravimetrically for mass concentrations as well as by Proton Elastic Scattering Analysis (PESA) and X-ray Fluorescence (XRF) for elemental concentrations (H, Na-Pb). Soil mass concentrations are estimated from measured elemental concentrations using the formula [*Malm et al.*, 1994]:

$$[SOIL] = 2.20[Al] + 2.49[Si] + 1.63[Ca] + 2.42[Fe] + 1.94[Ti] \quad (1)$$

[21] This formula is based upon the assumptions that FeO and Fe_2O_3 are equally abundant in the soil, and that the soil mass can be determined by summing the masses of the constituent oxides. Correction factors for other soil materials are also included in the coefficients. In the IMPROVE database, equation (1) is applied only to calculation of fine

soil mass concentrations, because the PM_{10} filters are not routinely analyzed for elemental composition; only PM_{10} gravimetric mass concentrations are reported. For INSPECT-II, however, elemental concentrations were obtained from the SPL PM_{10} filters and we applied equation (1) to estimate both $PM_{2.5}$ and PM_{10} soil mass concentrations.

[22] The nylon filters were extracted in water and analyzed via ion chromatography (IC) to determine the concentrations of nitrate, chloride, sulfate and nitrite ions. The quartz filters were analyzed for carbon using the Thermal Optical Reflectance (TOR) combustion method [*Chow et al.*, 1993]. The IMPROVE experimental apparatus and the methods for analysis are discussed in depth by *Malm et al.* [1994, 2004]. A similar sampler has operated since 1994 (24-hour samples at 3 day intervals) at Buffalo Pass in the Mt. Zirkel wilderness, 15 km to the northeast at a slightly higher elevation (3243 m MSL; Figure 1). Data from this sampler were used to compare bulk aerosol chemical composition from previous years with those measured in INSPECT-I. Archived IMPROVE data are available from http://vista.cira.colostate.edu/views/.

[23] Results of IMPROVE analyses of the SPL filters are compared with data from several other IMPROVE sites across the western United States during the INSPECT-II study period (locations shown in Figure 1). Because of their remote locations, the compositions of aerosols sampled at these sites are expected to reflect primarily regional influences. In contrast to the other sites chosen for this study, Kalmiopsis, on the Oregon coast, lies at a significantly lower elevation and is likely to have a stronger marine influence.

2.2.4. Transmission Electron Microscopy (TEM)

[24] During periods when ice crystals from the outlet of the CFDC were not being sampled by PALMS, they were collected via impaction onto carbon-coated Formvar films supported by Au TEM grids. TEM analyses was performed by the RJLee Group, Inc. (Monroeville, PA) using a JEOL Model 2000FX equipped with an Advanced Analysis Technologies light element energy dispersive spectrometer. Particles collected onto the Formvar film were examined directly in the TEM. The TEM focuses the electron beam transmitted through the specimen creating an image at an increased magnification onto a fluorescent screen. An initial evaluation of each grid was performed by scanning from one end of the grid to another in multiple directions at a relatively low magnification of $\sim$1000$\times$ to identify regions of particle impact. The TEM analysis was then conducted at magnifications ranging from 20k$\times$ to 85k$\times$ to provide information on individual particle size and elemental composition, concentrating on significant impaction areas, if detected. A minimum of 50 particles were examined per sample and micrographs of each particle were recorded to illustrate morphological characteristics. Particles were subsequently measured for maximum and minimum diameter using an image analysis program (AnalySIS). Particles observed primarily measured between 10 and 1000 nm. An energy dispersive spectrum was also acquired for each particle and in some cases for separate features within particles. Background spectra acquired from particle-free areas indicate the presence of carbon and oxygen (from the support film), copper and gold (from the TEM grid), and silicon (from an unknown source within the TEM). Therefore identification of these elements in particles can be problematic in some cases; however, minerals were distinguished on the basis of significantly higher levels of silicon compared to background spectra, and particles generating only spectral peaks comparable to the background spectra were classified as carbonaceous.

2.3. Supplementary Analyses

2.3.1. Back Trajectories

[25] Hourly back trajectories covering the entire campaign were generated using NOAA's HYbrid Single-Particle Lagrangian Integrated Trajectory (HYSPLIT) model in combination with the EDAS meteorological data set (http://www.arl.noaa.gov/ready/hysplit4.html) [*Draxler and Hess*, 2004]. The horizontal resolution of the EDAS data set is 40 km and the vertical resolution is 25 hPa. The domain of the EDAS data set covers the United States. Model vertical velocity is specified using the meteorological data. Trajectories were calculated for an arrival height of 500 m above SPL and terminated when they reached the EDAS boundary or after 5 days.

2.3.2. NAAPS

[26] The Navy Aerosol Analysis and Prediction System (NAAPS) was run for 2004 and the time-dependent vertical distribution of dust over the $1^\circ \times 1^\circ$ grid box containing SPL was extracted (http://www.nrlmry.navy.mil/aerosol/Docs/nrlmryonrprop.html). The Navy Operational Global Atmospheric Prediction System (NOGAPS), which has a horizontal spatial resolution of one-by-one degree and a temporal resolution of 6 hours, drives the meteorology in NAAPS. In NAAPS, dust emission rates are functions of the friction velocity, land use type, erodable fraction and soil moisture. Dust mass representing particles with diameters smaller than 10 microns (PM_{10}) are emitted into the lower two model layers according to *Westphal et al.* [1988].

3. Results

[27] Ice nucleation experiments began on 14 April and were completed on 19 May, with no aerosol data for the periods 22–26 April and 4–16 May. Measurements were conducted only in cloud-free conditions. During the late evening and early morning hours, the boundary layer inversion typically subsided with cooling of the surface such that the laboratory would reside in the free troposphere. As found by *Lowenthal et al.* [2002], the minimum hourly median value of CN concentrations typically occurred between 0800 and 0900 LST and were less than 2000 cm^{-3}. These concentrations are representative of remote continental background aerosol [*Seinfeld and Pandis*, 1998].

[28] Binned IN concentrations from INSPECT-I and II are shown as a function of water supersaturation (SS_w), ice supersaturation (SS_i), and temperature (T_a) in Figure 3. Data were divided into 20 bins covering the thermodynamic ranges of the measurements. The error bars represent the 95% confidence intervals for the mean value in the bins. Data collected above water saturation for both campaigns are excluded from this analysis; Figure 3 thus presents the data of greatest relevance to typical clouds in the mixed-phase cloud regime (i.e., cloud water supersaturations rarely exceeding 1%). During INSPECT-II, binned average [IN]

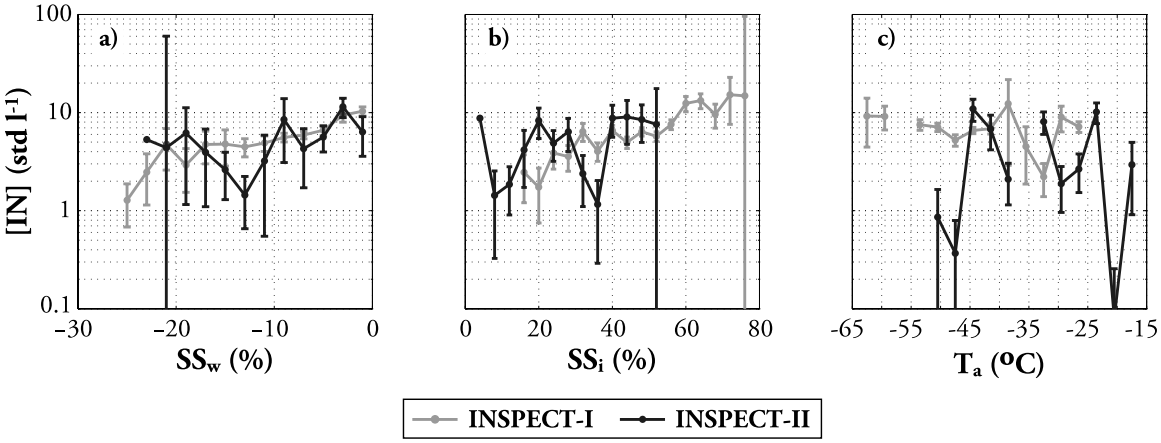

Figure 3. Binned average IN concentrations as a function of sample processing conditions: (a) supersaturation with respect to water, SS_w; (b) supersaturation with respect to ice, SS_i; and (c) temperature of aerosol lamina, T_a. Bars represent the 95% confidence intervals for the average values.

ranged from less than 1 to 10 per liter, similar to the concentrations reported by *DeMott et al.* [2003a] during INSPECT-I. However, [IN] showed more variability in INSPECT-II than observed during the first campaign, as indicated by the error bars.

[29] Figure 4 shows a box plot of [IN] data for several heterogeneous nucleation experimental periods with integrated ambient number concentrations ($D_p \geq 100$ nm) for the corresponding time periods. Figure 4a shows only those periods with sampling times exceeding 40 min under heterogeneous nucleation conditions in the CFDC; this makes the data statistically comparable. Despite low average [IN], median [IN] concentrations for several experimental periods were significantly enhanced relative to the median concentrations for other periods. These periods all occurred in April: midday on 15 April, the evening of

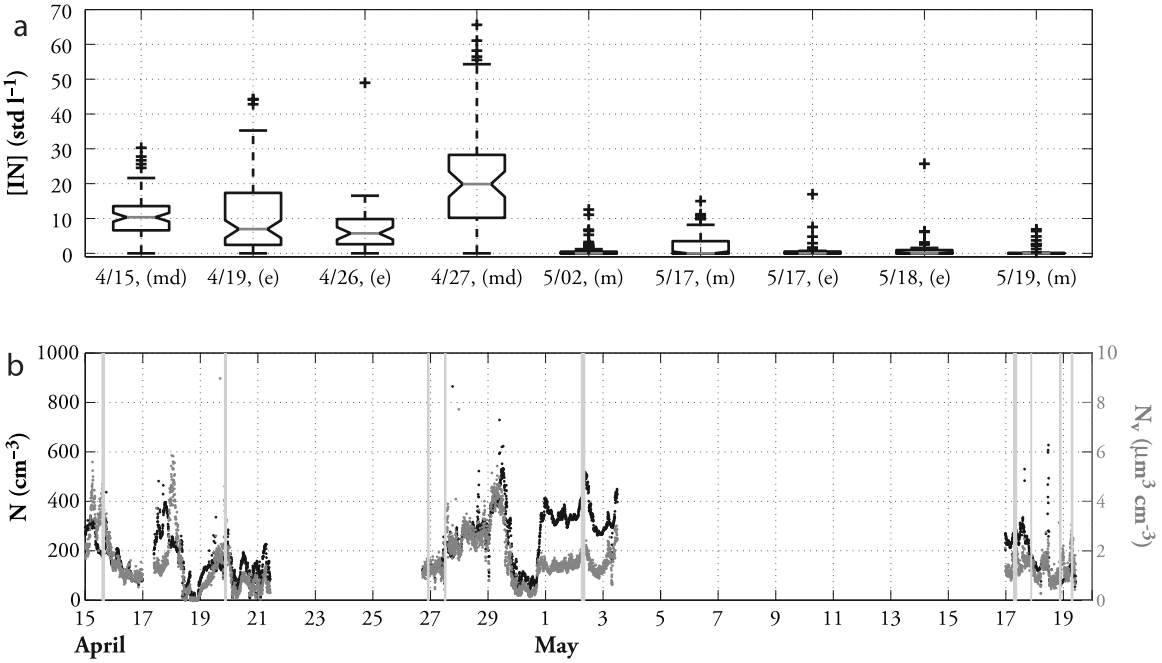

Figure 4. (a) Box and whisker plot of heterogeneous nucleation data for each sampling period. The identifiers "m," "md," and "e" stand for morning, midday, and evening, respectively. Horizontal box lines represent lower quartile, median and upper quartile values while the notches represent a robust estimate of the uncertainty about the medians in a box-to-box comparison. Boxes for which the notches do not overlap have medians that differ at the 95% confidence level. The whiskers indicate 1.5 times the interquartile range of the data while the crosses represent outliers in the data. Experimental periods shown in this plot are those for which at least 40 min of data were obtained. (b) OPC integrated number and volume concentrations ($D_p \geq 100$ nm). The solid bars in Figure 4b represent the experimental periods shown in Figure 4a.

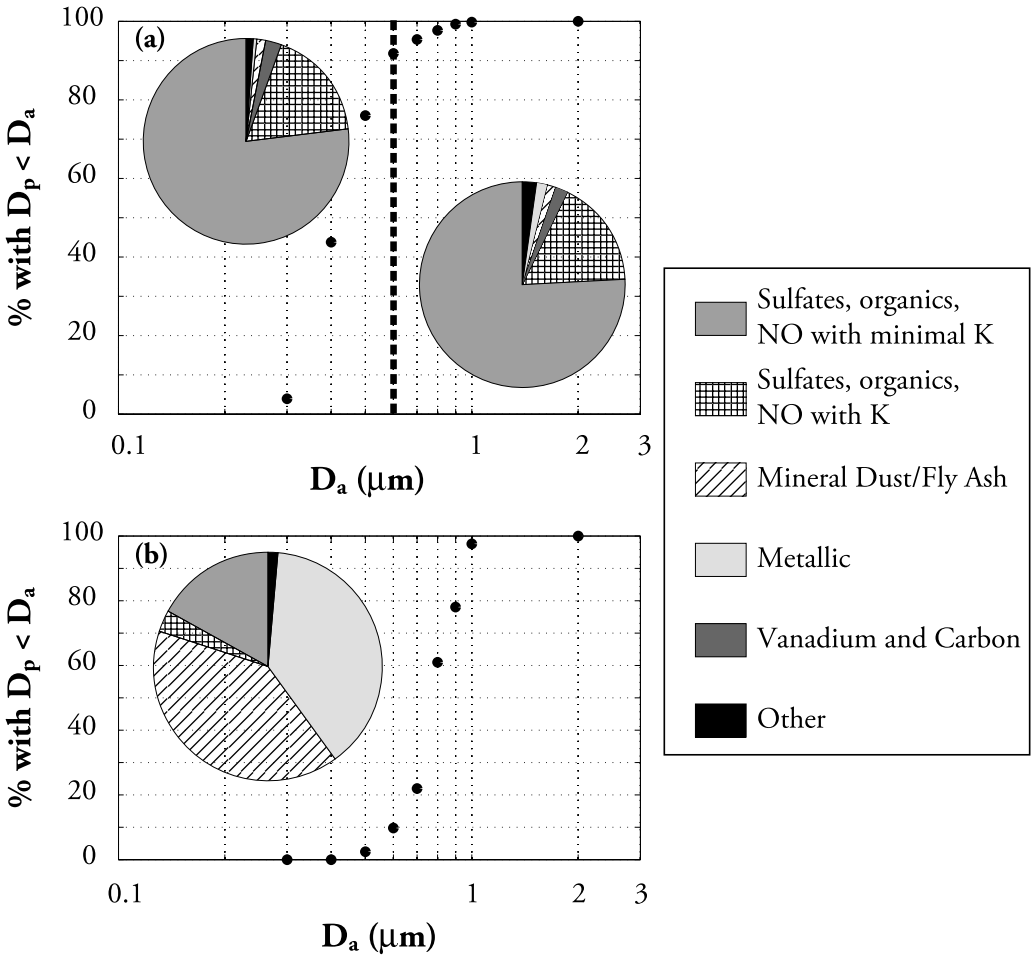

Figure 5. Composition and sizes of particles (a) in the ambient population and (b) those that serve as ice nuclei, as determined by PALMS. Left insets in both panels show fractional compositions for the total population sampled. The right inset in Figure 5a shows the composition of ambient particles with sizes larger than 0.6 microns (indicated by the dashed line).

19 April, and midday on 27 April. Figure 4b shows that variations in the number concentrations of particles with $D_p \geq 100$ nm are generally, but not always, consistent with these variations in [IN].

[30] These periods of elevated [IN] during this campaign correlate well with periods of elevated soil dust aerosol concentrations. These results are not surprising; as in INSPECT-I [*DeMott et al.*, 2003a], PALMS data reveal that IN composition is dominated by mineral dust/fly ash and metallic particle categories (Figure 5). In contrast, the predominant particle composition category (>75%) for ambient particles is mixed sulfates and organics.

[31] In addition to particle composition, PALMS included the capability to measure the aerodynamic diameter of transmitted particles, a measurement not available for the previous campaign. The size data indicate a sharp distinction between the average size of an ambient particle and that of a particle serving as an IN. PALMS measured a median aerodynamic diameter of ~0.75 μm for IN; all but one particle for which a diameter was retrieved had a diameter greater than or equal to 0.5 μm. In contrast, PALMS measured a median aerodynamic diameter of ~0.42 μm for ambient particles. The lower-right corner of Figure 5a shows the composition of ambient aerosol with aerodynamic diameters greater than 0.6 microns (as indicated by the dashed line in Figure 5a); the composition of these particles is similar to that found in the total ambient aerosol, indicating that the observed differences in composition between IN and the ambient aerosol are not solely a result of size-dependent composition variations.

4. Discussion

4.1. Evidence for Dust

[32] As indicated in the previous section, insoluble material such as metals and mineral dusts appear to dominate IN composition. Therefore high [IN] events are expected to correlate with periods during which soil dust dominates the aerosol composition. Figure 6 shows several indicators of soil dust contributions at SPL. Figure 6a contains NAAPS model output as a function of height for the grid box in which SPL is located. The NAAPS model predicted sustained and elevated dust surface concentrations for two periods (15–18 April and 26–29 April) during INSPECT-II. In both cases, the dust arrived first in the upper levels of the atmosphere then at decreasing heights until it reached the surface over a period of

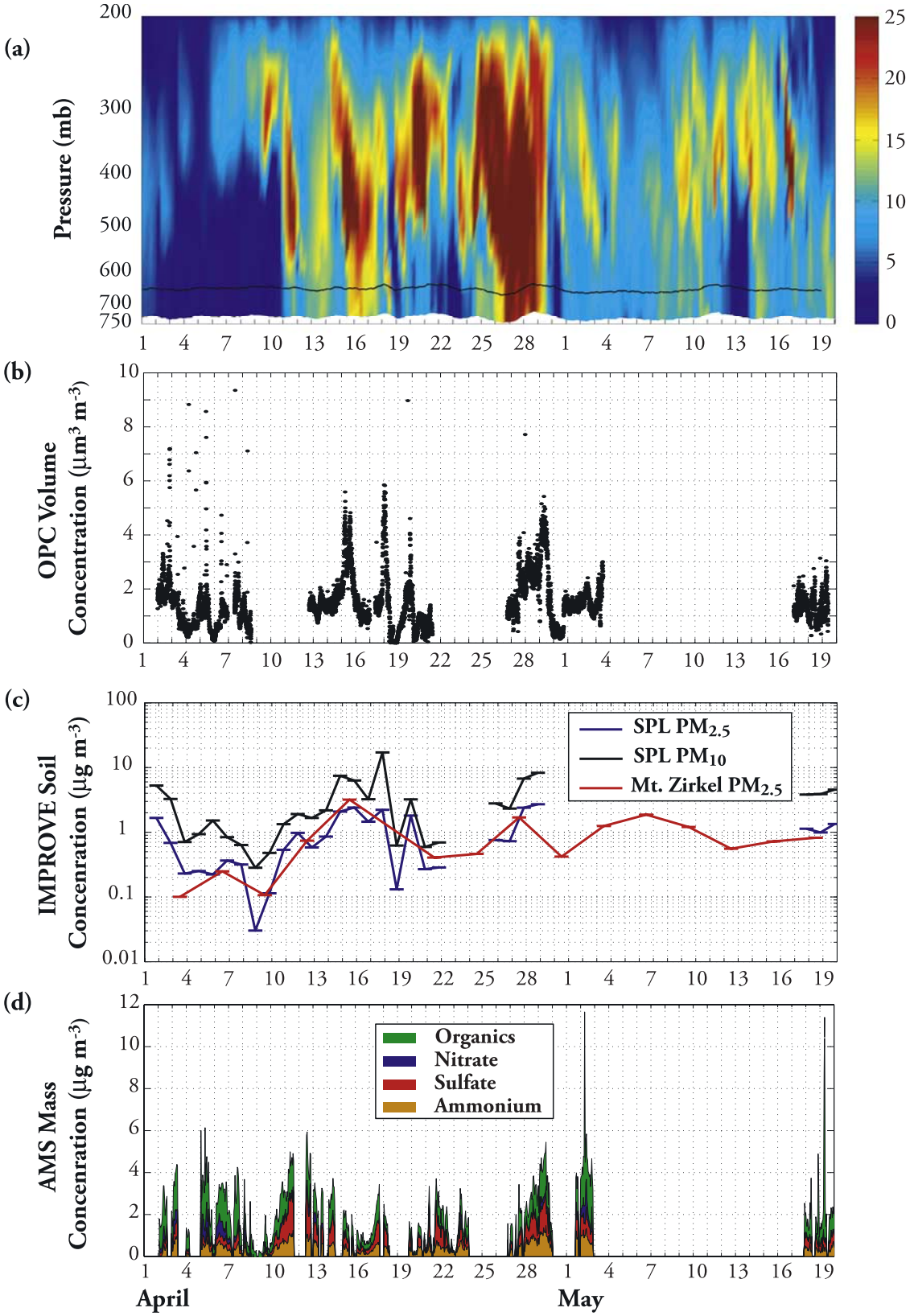
(a)
Pressure (mb)
200
300
400
500
600
700
750
25
20
15
10
5
0
(b)
OPC Volume Concentration (μm³ m⁻³)
(c)
IMPROVE Soil Concenration (μg m⁻³)
SPL PM2.5
SPL PM10
Mt. Zirkel PM2.5
(d)
AMS Mass Concenration (μg m⁻³)
Organics
Nitrate
Sulfate
Ammonium
April
May

Figure 6

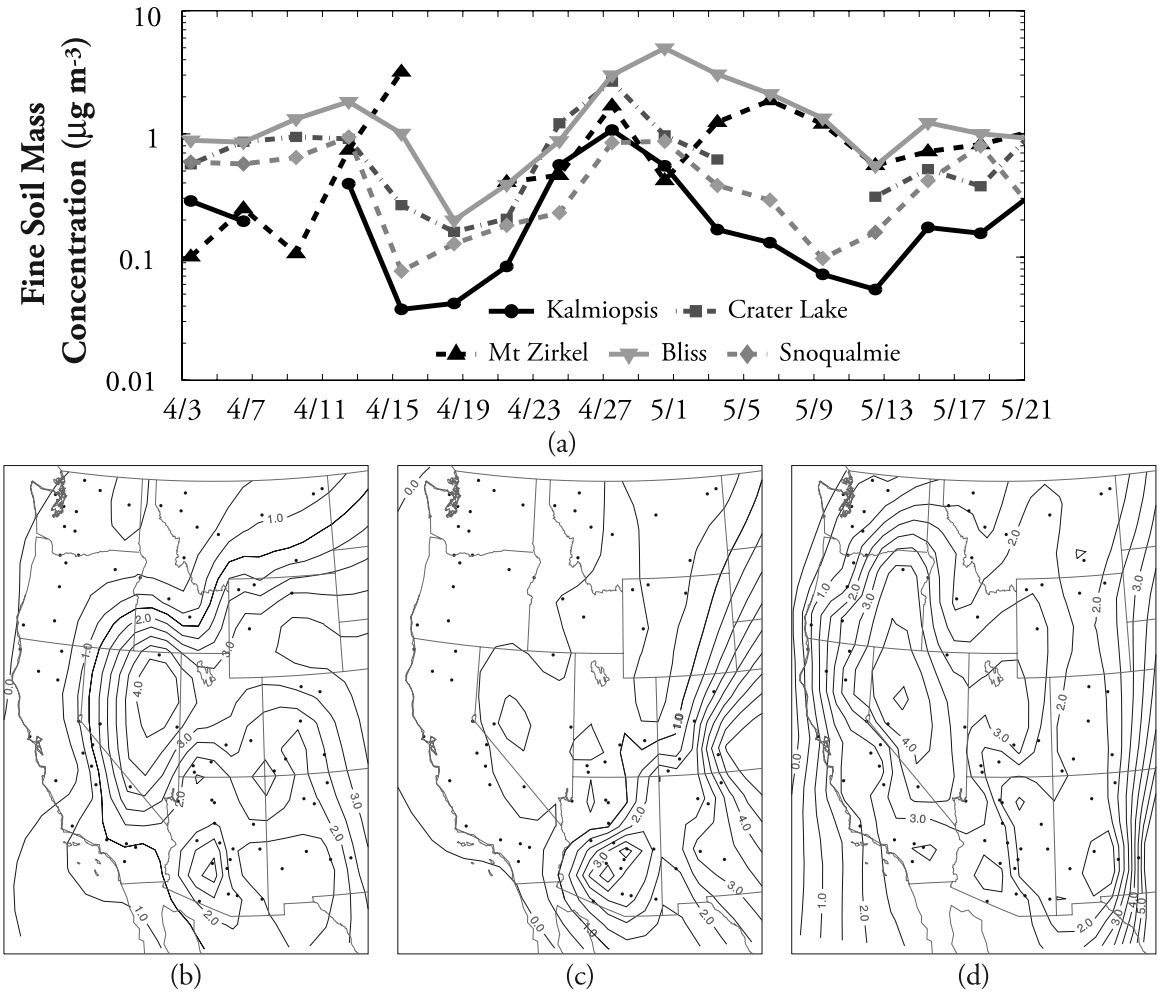

Figure 7. IMPROVE fine soil mass concentrations for sites across the western United States. (a) Timeline of fine soil mass concentrations at the IMPROVE sites shown in Figure 1. Snapshots of fine soil mass concentrations (μg m^{-3}) across the western portion of the IMPROVE network for (b) 15, (c) 18, and (d) 27 April. The dots on the map indicate the locations of the IMPROVE network sites used to construct the contours.

several days. The first event started around noon of 15 April and continued through 17 April, after which a front passed through and particle concentrations dropped dramatically throughout 18 April.

[33] The first observation of elevated [IN], midday on 15 April, occurred during this predicted dust event. During this period, the daily IMPROVE data at SPL (Figure 6c) indicate elevated fine ($PM_{2.5}$) soil mass concentrations (>1 μg m^3) for each day. The particle volume concentration estimated from OPC size distributions (Figure 6b) decreased through 16 and 17 April, during which there was a period of higher surface pressures. Beginning in the evening of 17 April, surface pressure began to drop and particle volume concentrations increased dramatically for a brief period. IMPROVE PM_{10} soil mass concentrations, which include contributions from both the fine and coarse mode soil, reached their highest values for the entire campaign (almost 20 μg m^{-3}) during this period.

[34] NAAPS predicted the occurrence of a similar but more intense dust event toward the end of April. Observed particle volume concentrations (Figure 6b) began rising on 26 April and continued to rise until the morning of 29 April. Once again, particle volume concentrations reached their peak as the pressure began to drop and prior to the passage of a front. NAAPS predicted the largest surface concentrations of dust in the SPL grid during this period; however, other measures of dust concentrations indicate that this event was similar in intensity to the event on 15 April.

Figure 6. Predicted and measured indicators of dust concentrations and aerosol composition during the period covered by the campaign. (a) NAAPS predictions of dust concentrations (μg m^{-3}) at a grid box centered at 106.5°W, 40.5°N as a function of height. The black line indicates surface pressure recorded at the laboratory. (b) Integrated particle volume concentration for optical diameters larger than 0.1 μm. (c) IMPROVE fine ($PM_{2.5}$) and total (PM_{10}) soil mass concentrations recorded at SPL and the fine soil mass concentration recorded at Mt. Zirkel. (d) AMS mass concentrations of major nonrefractory aerosol constituents. Data are plotted cumulatively (i.e., the organics line indicates the total mass concentrations observed).

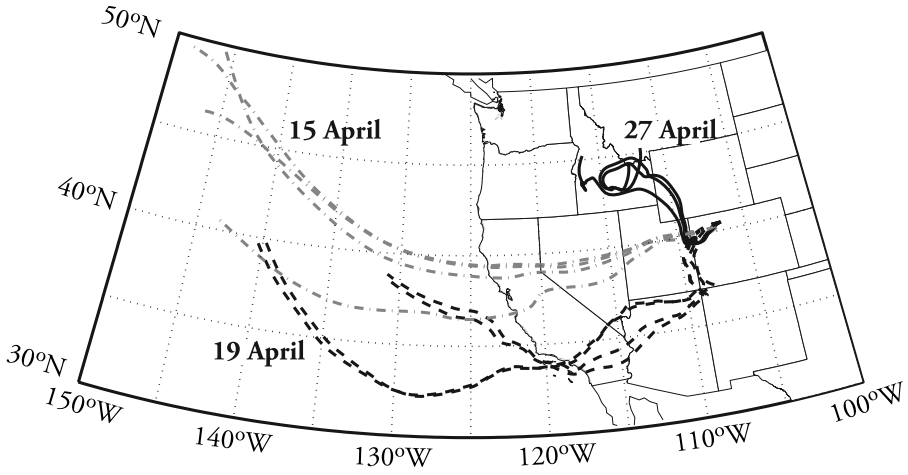

Figure 8. Five day back trajectories covering the experimental periods for which there were significantly elevated [IN] (15, 19, and 27 April).

The CFDC measured the highest median [IN] for the study during this event (midday 27 April; Figure 4a).

[35] [IN] on 19 April also appear to be significantly greater than the median study value. In contrast to the previously described events, NAAPS predicted only slightly elevated surface soil dust concentrations during the latter part of the day. The SPL IMPROVE samples indicate relatively high fine soil mass concentrations ($\sim$2 μg m^{-3}; Figure 6c) and only a small contribution from coarse-mode dust. Particle volume concentrations increased monotonically from the morning of 19 April until the evening, when moisture arrived on the edge of a short-wave trough. This event, though short in duration, is similar to the others as elevated fine soil mass concentrations were associated with a deepening trough.

[36] Further analysis of IMPROVE network data combined with the back trajectories provides some insight into the nature of the dust transport. During the sample period covering 15–18 April, IMPROVE sites across the western United States indicate elevated concentrations of soil (Figure 7a). Consistent with *VanCuren and Cahill* [2002], the higher-altitude sites tended to see higher fine soil concentrations. On 12 April, all sites shown in Figure 1 west of Mt. Zirkel measured peaks in their fine soil concentrations. Mt. Zirkel and Bliss State Park both showed elevated (>1 μg m^{-3}) mass concentrations of fine soil on 15 April, by which date the northwestern sites no longer recorded high concentrations. Back trajectories for 15 April (Figure 8) also indicate that air parcels reaching SPL originated due west of the laboratory. These observations suggest a plume entering the western United States and then moving east toward SPL. Similarly, *Zhao et al.* [2006] found that Asian dust is typically transported zonally (centered at 40°N) at altitudes of 3 to 10 km.

[37] Similar to the mid-April event, IMPROVE samplers across the western United States measured elevated concentrations of fine soil during the event covering 26 to 29 April. These measurements were also sorted by sample location, with the highest sites measuring the highest concentrations. However, the timing of peak dust concentrations at various sites differed more for the mid-April event than the late-April event. All IMPROVE sites in Figure 1 measured elevated fine soil mass concentrations on 27 April (Figure 7a). In fact, IMPROVE sites across the western United States measured elevated fine soil concentrations for this day (Figure 7d), suggesting this was a widespread fine soil incursion. During this period, a large ridge was situated over the western portion of the United States. The influence of the ridge on lower level back trajectories is evident in Figure 8: trajectories remain near the surface in the region of the laboratory for life of the trajectories (5 days). However, trajectories calculated for an arrival height above 2 km (not shown) exit the model boundary west of the laboratory in approximately 3.5 days.

[38] The widespread nature of the events described above and the increase in measurable fine soil mass with altitude suggests that elevated soil concentrations may be attributable to long-range transport from eastern Asia. Indeed, in NAAPS large events such as these are attributed almost solely to Asian outflow. In contrast, measurements occurring about the 19 April experiment indicated that the nature of the dust incursion was different than the 15–18 and 26–29 April events. The event on 19 April was shorter in duration, with SPL in-cloud much of the day. Back trajectories during the 19 April sampling period indicate that air parcels arriving at the laboratory passed through a particularly arid region of the United States (Figure 8). IMPROVE data for sites located in southwestern Colorado, New Mexico and Arizona southwest of the laboratory show elevated fine soil mass concentrations at all elevations just prior to the event at SPL (18 April, Figure 7c) while there was no corresponding increase in the fine soil concentration at other western IMPROVE sites (Figure 7a). PALMS cluster analyses provided a measure of the fractions of ambient particles sampled ($\sim$0.3 to 1 μm) that contained mineral dust (or fly ash) and those that contained metals, that may also reflect dust sources at times. Project-average fractions in the mineral dust/fly ash and metal cluster categories around IN sampling times were 1.5% and 0.7%. The percentage contributions on 19 April of 3.9% and 3.2% were the only ones that were significantly higher than the mean at the 95% confidence level. Although this observation does not definitively demonstrate a different source of particulate matter to SPL on this day, it does

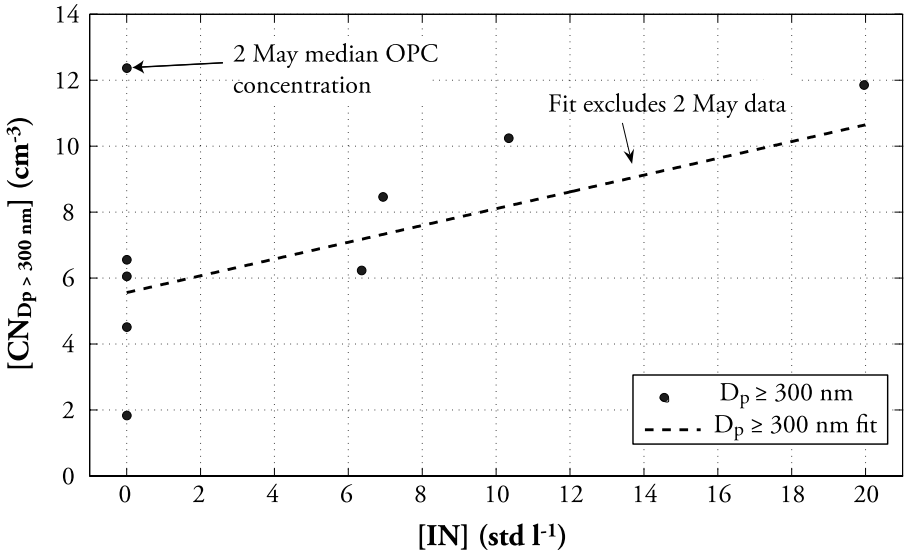

Figure 9. Median concentrations of particles with $D_p > 300$ nm versus median [IN]. The line represents a linear fit to the data (excluding the 2 May point) and has an r^2 of ~0.77.

provide additional evidence for a more regional dust source on 19 April that led to higher concentrations of suspended mineral dust particles in the 0.3 to 1 μm size range.

[39] Although fine soil concentrations at other IMPROVE sites in the southwestern United States combined with the back trajectory analysis suggest a regional source of dust on 19 April, it is possible that dust from both long-range transport and regional sources is present at SPL. Currently, there are no proposed methodologies using elemental chemical composition by which one can easily differentiate between dust emanating from arid regions in the western United States and dust from the deserts of eastern Asia. Indeed, *VanCuren and Cahill* [2002] limited their analysis to north and midwestern IMPROVE sites because of the difficulty in deconvolving east Asian dust from western U.S. dust.

4.2. IN Activity Relation to the Aerosol Distribution

[40] The role of dust particles as ice nuclei would suggest that there might be an inherent relation between occurrences of increased concentrations of larger aerosol particles and increased concentrations of IN; a relation that might be exploited for use in numerical modeling of global IN distributions and impacts. Such relations have been noted in some cases previously, without reference to the role of dust particles [*Berezinskii et al.*, 1986; *DeMott et al.*, 2003a; *Georgii and Kleinjung*, 1967].

[41] Although Figure 4 suggests there may be correlation between [IN] and concentrations of accumulation mode aerosol, it is clear that data from the 2 May experiment confound a clear correlation. As on days with high [IN], during the experiment of 2 May there was a large increase in the number concentrations of particles with $D_p \geq 100$ nm (Figure 4b); however, there was no corresponding increase in [IN]. Considering that most IN appear to have somewhat larger sizes, we used a more stringent size limitation for directly correlating IN and aerosol concentrations. In Figure 9, the concentrations of particles with $D_p \geq 300$ nm are directly compared to [IN] for the different experimental periods. A linear correlation between aerosol and IN is evident above some threshold value for aerosol concentrations (~5 cm^{-3}). However, a higher correlation coefficient is still only achieved if the data point associated with 2 May is excluded. Correlations with larger ranges of aerosol sizes were not explored because the experimental limitation on sampling IN precluded determining the IN contribution from particles larger than 1 μm.

[42] We believe that a particular pollution episode was responsible for causing elevated concentrations of accumulation mode particles on 2 May and that these particles were either poor IN or the presence of pollutants affected IN negatively on this day. Measurements of sulfur dioxide concentrations ([SO_2]) and ozone concentrations ([O_3]) indicated elevated levels of anthropogenic pollution. [SO_2] on the morning of 2 May peaked at over an order of magnitude higher than the median (170 ppt for clear-sky conditions), and remained elevated throughout the day. On this day, the AMS measured mass concentrations that reached a factor of two higher than other periods (Figure 6d). Nitrates and organics dominated these measurements with unusually high concentrations of both species. The TEM analyses of the ambient aerosol from samples taken just prior to this event and nearly coincident with the IN sampling period (Figures 10c and 10d) show the two predominant particle types present. One type was dominated by spherical silicates, some with soot also present, suggestive of outflow from an industrial combustion process [*Vassilev et al.*, 2001]. Another type contained carbon and potassium and was coated by significant amounts of sulfur. As demonstrated in the TEM images (Figures 10c and 10d) ambient particles were typified by compositions and morphological characteristics indicative of combustion processes and in some cases were heavily coated. In comparison, activated IN examined in TEM analyses were relatively free of coatings (Figures 10a and 10b). Most IN were irregular particles of the type shown in Figure 10a that may come from soil dust, while a few, such as the soot agglomerate shown in Figure 10b, had an apparent combustion source.

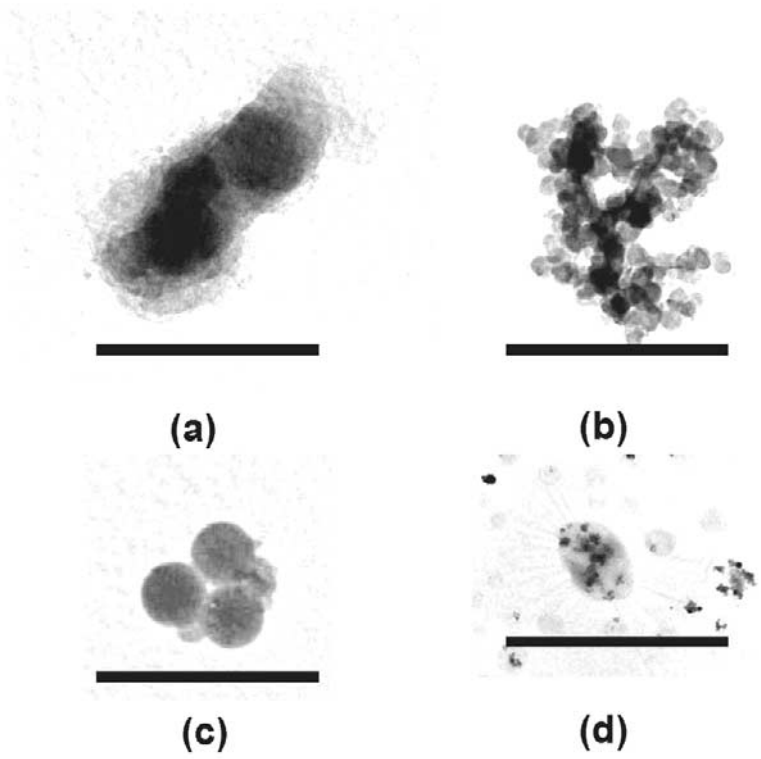

Figure 10. TEM images from the 2 May experiment. Solid bars represent 500 nm. (a) Ice nucleus containing predominantly (in order) silicon, aluminum and oxygen with minor amounts of potassium and iron, identified as a mineral dust particle with little or no associated sulfur. (b) Ice nucleus composed of relatively pure carbonaceous soot. (c) An ambient particle agglomerate of amorphous spheres with diameters of ~150 nm. The particles had major elemental signatures for Si and O, with modest amounts of Mg, Na, S, and K also present. This composition and morphology may be associated with fly ash. (d) Ambient particles composed primarily of large amounts of carbon, sulfur, and potassium that typified a large class of the aerosol on 2 May.

[43] These findings indicate that enhancements in the number concentrations of accumulation mode particles are not necessarily indicative of enhancements in [IN]. Rather, IN activity is more appropriately determined by the physical and chemical characteristics of the individual particles. Although a parameterization of IN activity based on some portion of the aerosol population would be quite useful for modeling studies, on the basis of these results this parameterization has the potential to overpredict [IN] in certain cases. Linking IN parameterizations to known source aerosols such as mineral dusts may be the best strategy. In this regard, it will be important to conduct further investigations of the potential positive and negative impacts of pollution on IN populations.

5. Summary and Conclusions

[44] From the analysis of the 15 and 27 April elevated-dust-concentration events, we can make several observations concerning their nature. On the basis of the NAAPS analysis, it appears that dust layers from long-range transport having a measurable impact on surface aerosol soil concentrations typically arrive first in the upper atmosphere and then at lower altitudes until measurable dust concentrations reach the surface after several days. These layers are associated with troughs, and we infer that surface soil concentrations tend to reach their peak values immediately preceding any precipitation associated with these troughs. As these dust layers reached SPL, we observed elevated [IN]. This is consistent with laboratory observations that mineral dust particles are well suited to serve as IN [e.g., *Archuleta et al.*, 2005].

[45] The apparent dust event that occurs on 19 April, although also associated with elevated [IN], may be different than the other events. First, it is shorter in duration. The event occurs between two tightly spaced fronts and in the presence of a short-wave trough. Because of the timing of the IMPROVE filter rotations, there is no other record of this event upstream of the laboratory on this day. The trajectory paths for the CFDC sampling period are also different than those of the other events. On the basis of the HYSPLIT analysis, air parcels appear to pass over a particularly arid region of the United States. This region was identified by *Prospero et al.* [2002] as a source region for atmospheric mineral dust during this time of year. Because of the limited regional dust data available during

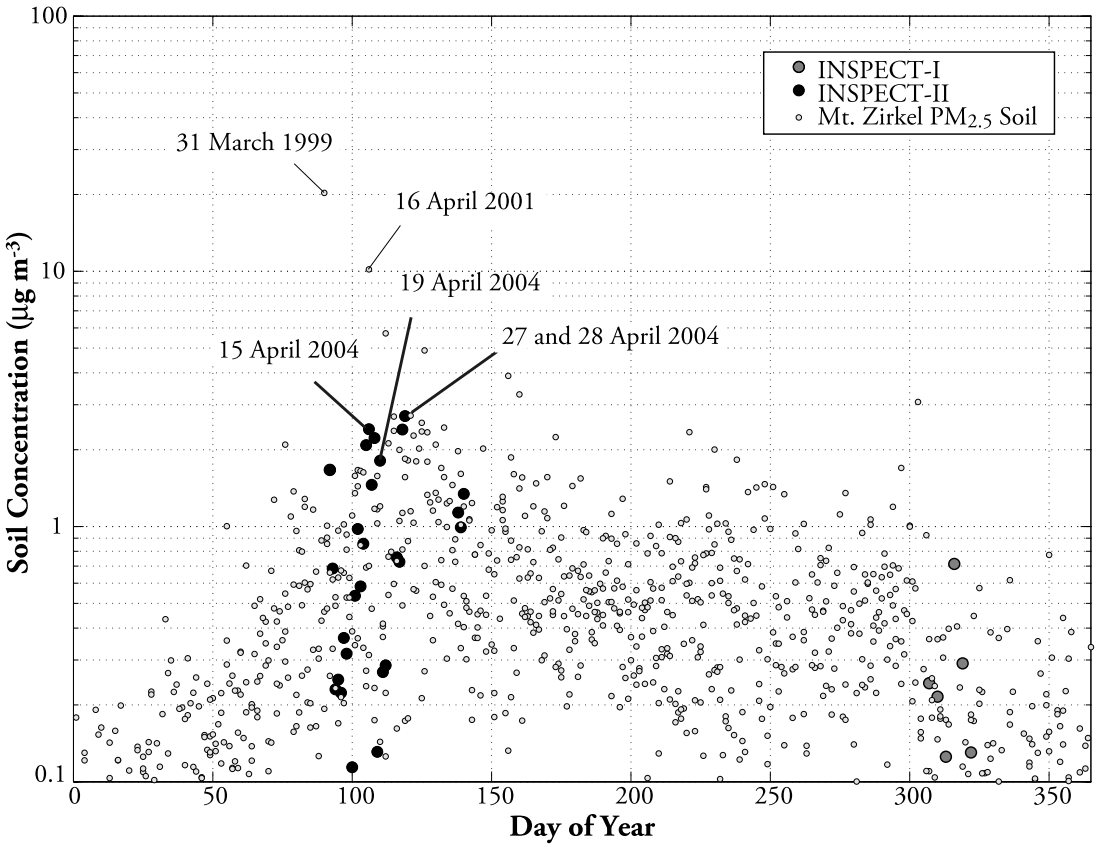

Figure 11. Comparison of IMPROVE fine soil concentrations measured at SPL during INSPECT-II with those in the historical record from the nearby Mt. Zirkel site (30 July 1994 to 29 December 2004). The grey solid circles are data collected during the period of INSPECT-I (1 to 19 November 2001) as measured at the Mt. Zirkel site. The two largest dust concentrations recorded at Mt. Zirkel are coincident with Asian dust outbreaks in the spring of 1999 [*Ogunjobi et al.*, 2003] and the spring of 2001 [*Kahn et al.*, 2004; *Kalashnikova et al.*, 2005].

this event, and the possibility that the air mass originated in the western Pacific and was transporting Asian dust, it is difficult to assign source regions for the soil observed during this event.

[46] *Perry et al.* [2004] and *Ooki and Uematsu* [2005] suggest that through interactions with polluted air masses (emanating from the eastern coast of Asia), dust particles originating from the arid regions of China may become coated with nitrates and sulfates. Soluble coatings on IN would potentially alter ice nucleation mechanisms, inhibiting nucleation by vapor deposition and favoring condensation-freezing nucleation. The impact on ice nucleation efficiency is unclear. On the basis of the results from the CFDC analysis (Figure 3), there appears to be no remarkable increase in IN activity with SS_w. Further, the PALMS IN compositional data do not indicate significant contributions from soluble material. We thus conclude that most of the dust-related IN during this campaign were not coated with measurable amounts of soluble material. In a noted pollution case, the IN population did not include particles of an industrial nature that were coated with solutes although the ambient population had many such particles in the size range typical of IN. Thus a consideration should be given in future research to the possibility that particle coatings may act to either enhance or poison ice nucleation efficiency.

[47] Figure 11 presents a summary of the fine soil mass concentrations at SPL during INSPECT-II, as estimated from the IMPROVE data, compared with those in the historical record from the Mt. Zirkel site. Dust mass concentrations during INSPECT-II are only slightly higher than those during INSPECT-I. The INSPECT-II values span most of the range of the longer-term record, but do not reach the highest springtime values seen in some years (e.g., the 31 March 1999 and 16 April 2001 events). If, as our data suggest, dust is a significant source of IN, and [IN] vary with dust concentrations, we may conclude that the range of [IN] observed in INSPECT-II in 2004, $1-10$ std l^{-1}, is typical of surface concentrations in most years. However, in years with strong Asian dust transport, the dust concentrations can be increased 10-fold. We thus expect that [IN] would also increase, although the correlation is not necessarily linear. Also, as seen in Figure 6a, dust concentrations aloft may be significantly higher than those observed at an elevated surface site, which means that [IN] at altitudes relevant to cold cloud formation may be underestimated by our observations. Finally, as our data are not corrected for sampling losses and do not include IN larger than 1 micron, they are expected to be conservative estimates of the actual ambient [IN] active at the processing T and RH.

[48] **Acknowledgments.** We thank Piotr Flatau, Marcin Witek, and Kelley Johnson for use of the NAAPS model and assistance with the analysis of the output. We appreciate Dan Murphy's assistance with NOAA's PALMS instrument and data. We thank William Malm, Chuck McDade, and John Faust of Air Resource Specialists for their support in obtaining and analyzing the IMPROVE samples. This research was supported by the National Science Foundation, grants ATM-0334228 and ATM-0334308. Logistical assistance from the Steamboat Ski and Resort Corporation is greatly appreciated. DRI is an equal opportunity service provider and employer and is a permittee of the Medicine-Bow and Routt National Forests.

References

Allan, J. D., J. L. Jimenez, P. I. Williams, M. R. Alfarra, K. N. Bower, J. T. Jayne, H. Coe, and D. R. Worsnop (2003), Quantitative sampling using an Aerodyne Aerosol Mass Spectrometer: 1. Techniques of data interpretation and error analysis, *J. Geophys. Res.*, *108*(D3), 4090, doi:10.1029/2002JD002358.

Archuleta, C. M., P. J. DeMott, and S. M. Kreidenweis (2005), Ice nucleation by surrogates for atmospheric mineral dust and mineral dust/sulfate particles at cirrus temperatures, *Atmos. Chem. Phys.*, *5*, 2617–2634.

Augustine, J. A., J. J. DeLuisi, C. R. Cornwall, G. B. Hodges, C. N. Long, and C. I. Medina (2003), An automated method of MFRSR calibration for aerosol optical depth analysis with application to an Asian dust outbreak over the United States, *J. Appl. Meteorol.*, *42*(2), 266–278, doi:10.1175/1520-0450(2003)042<0266:AAMOMC>2.0.CO;2.

Berezinskii, N. A., G. V. Stepanov, and V. G. Khorguani (1986), Altitude variation of relative ice-forming activity of natural aerosol, *S. Meteorol. Hydr.*, *12*, 86–89.

Boulter, J., D. Cziczo, A. Middlebrook, D. Thomson, and D. Murphy (2006), Design and performance of a pumped counterflow virtual impactor, *Aerosol Sci. Technol.*, *40*, 969–976, doi:10.1080/02786820600840984.

Borys, R. D., and M. A. Wetzel (1997), Storm Peak Laboratory: A research, teaching, and service facility for the atmospheric sciences, *Bull. Am. Meteorol. Soc.*, *78*(10), 2115–2123.

Buck, A. L. (1981), New equations for computing vapor-pressure and enhancement factor, *J. Appl. Meteorol.*, *20*(12), 1527–1532.

Chen, Y. L., S. M. Kreidenweis, L. M. McInnes, D. C. Rogers, and P. J. DeMott (1998), Single particle analyses of ice nucleating aerosols in the upper troposphere and lower stratosphere, *Geophys. Res. Lett.*, *25*(9), 1391–1394.

Chen, Y. L., P. J. DeMott, S. M. Kreidenweis, D. C. Rogers, and D. E. Sherman (2000), Ice formation by sulfate and sulfuric acid aerosol particles under upper-tropospheric conditions, *J. Atmos. Sci.*, *57*(22), 3752–3766.

Chow, J. C., J. G. Watson, L. C. Pritchett, W. R. Pierson, C. A. Frazier, and R. G. Purcell (1993), The DRI thermal optical reflectance carbon analysis system–Description, evaluation, and applications in United States air-quality studies, *Atmos. Environ.*, *27*(8), 1185–1201.

Crow, E. L., F. A. Davis, and M. W. Maxfield (1960), *Statistics Manual*, Dover, Mineola, New York.

Cziczo, D. J., P. J. DeMott, C. Brock, P. K. Hudson, B. Jesse, S. M. Kreidenweis, A. J. Prenni, J. Schreiner, D. S. Thomson, and D. M. Murphy (2003), A method for single particle mass spectrometry of ice nuclei, *Aerosol Sci. Technol.*, *37*(5), 460–470, doi:10.1080/02786820390112687.

Cziczo, D. J., D. M. Murphy, P. K. Hudson, and D. S. Thomson (2004), Single particle measurements of the chemical composition of cirrus ice residue during CRYSTAL-FACE, *J. Geophys. Res.*, *109*, D04201, doi:10.1029/2003JD004032.

DeMott, P. J., D. J. Cziczo, A. J. Prenni, D. M. Murphy, S. M. Kreidenweis, D. S. Thomson, R. Borys, and D. C. Rogers (2003a), Measurements of the concentration and composition of nuclei for cirrus formation, *Proc. Natl. Acad. Sci. U. S. A.*, *100*(25), 14,655–14,660, doi:10.1073/pnas.2532677100.

DeMott, P. J., K. Sassen, M. R. Poellot, D. Baumgardner, D. C. Rogers, S. D. Brooks, A. J. Prenni, and S. M. Kreidenweis (2003b), African dust aerosols as atmospheric ice nuclei, *Geophys. Res. Lett.*, *30*(14), 1732, doi:10.1029/2003GL017410.

Draxler, R. R., and G. D. Hess (2004), Description of the HYSPLIT_4 Modeling System, 28 pp., report, Natl. Oceanographic and Atmos. Admin., Air Resour. Lab., Silver Spring, Md.

Georgii, E. W., and E. Kleinjung (1967), Relations between the chemical composition of atmospheric aerosol particles and the concentration of natural ice nuclei, *J. Rech. Atmos.*, *3*, 145–156.

Gierens, K. (2003), On the transition between heterogeneous and homogeneous freezing, *Atmos. Chem. Phys.*, *3*, 437–446.

Gilmore, M. S., J. M. Straka, and E. N. Rasmussen (2004), Precipitation and evolution sensitivity in simulated deep convective storms: Comparisons between liquid-only and simple ice and liquid phase microphysics, *Mon. Weather Rev.*, *132*, 1897–1916, doi:10.1175/1520-0493(2004)132<1897:PAESIS>2.0.CO;2.

Haag, W., and B. Kärcher (2004), The impact of aerosols and gravity waves on cirrus clouds at midlatitudes, *J. Geophys. Res.*, *109*, D12202, doi:10.1029/2004JD004579.

Heintzenberg, J., K. Okada, and J. Strom (1996), On the composition of non-volatile material in upper tropospheric aerosols and cirrus crystals, *Atmos. Res.*, *41*(1), 81–88, doi:10.1016/0169-8095(95)00042-9.

Husar, R. B., et al. (2001), Asian dust events of April 1998, *J. Geophys. Res.*, *106*(D16), 18,317–18,330.

Jayne, J. T., D. C. Leard, X. F. Zhang, P. Davidovits, K. A. Smith, C. E. Kolb, and D. R. Worsnop (2000), Development of an aerosol mass spectrometer for size and composition analysis of submicron particles, *Aerosol Sci. Technol.*, *33*, 49–70, doi:10.1080/027868200410840.

Jimenez, J. L., et al. (2003), Ambient aerosol sampling using the Aerodyne Aerosol Mass Spectrometer, *J. Geophys. Res.*, *108*(D7), 8425, doi:10.1029/2001JD001213.

Johnston, M. V. (2000), Sampling and analysis of individual particles by aerosol mass spectrometry, *J. Mass Spectrom.*, *35*(5), 585–595, doi:10.1002/(SICI)1096-9888(200005)35:5<585:AID-JMS992>3.0.CO;2-K.

Kahn, R., et al. (2004), Environmental snapshots from ACE-Asia, *J. Geophys. Res.*, *109*, D19S14, doi:10.1029/2003JD004339.

Kalashnikova, O. V., R. Kahn, I. N. Sokolik, and W. H. Li (2005), Ability of multiangle remote sensing observations to identify and distinguish mineral dust types: Optical models and retrievals of optically thick plumes, *J. Geophys. Res.*, *110*, D18S14, doi:10.1029/2004JD004550.

Kärcher, B. (2004), Cirrus clouds in the tropical tropopause layer: Role of heterogeneous ice nuclei, *Geophys. Res. Lett.*, *31*, L12101, doi:10.1029/2004GL019774.

Liu, C., M. W. Moncrieff, and E. J. Zipser (1997), Dynamical influence of microphysics in tropical squall lines: A numerical study, *Mon. Weather Rev.*, *125*, 2193–2210.

Lowenthal, D. H., R. D. Borys, and M. A. Wetzel (2002), Aerosol distributions and cloud interactions at a mountaintop laboratory, *J. Geophys. Res.*, *107*(D18), 4345, doi:10.1029/2001JD002046.

Malm, W. C., J. F. S. D. Huffman, R. A. Eldred, and T. A. Cahill (1994), Spatial and seasonal trends in particle concentration and optical extinction in the United States, *J. Geophys. Res.*, *99*(D1), 1347–1370.

Malm, W. C., B. A. Schichtel, M. L. Pitchford, L. L. Ashbaugh, and R. A. Eldred (2004), Spatial and monthly trends in speciated fine particle concentration in the United States, *J. Geophys. Res.*, *109*, D03306, doi:10.1029/2003JD003739.

Murphy, D. M., A. M. Middlebrook, and M. Warshawsky (2003), Cluster analysis of data from the Particle Analysis by Laser Mass Spectrometry (PALMS) instrument, *Aerosol Sci. Technol.*, *37*(4), 382–391, doi:10.1080/02786820390125241.

Ogunjobi, K. O., Y. J. Kim, and Z. He (2003), Aerosol optical properties during Asian dust storm episodes in South Korea, *Theor. Appl. Climatol.*, *76*(1–2), 65–75, doi:10.1007/s00704-003-0006-7.

Ooki, A., and M. Uematsu (2005), Chemical interactions between mineral dust particles and acid gases during Asian dust events, *J. Geophys. Res.*, *110*, D03201, doi:10.1029/2004JD004737.

Parrish, D. D., J. S. Holloway, and F. C. Fehsenfeld (1994), Routine, continuous measurement of carbon-monoxide with parts-per-billion precision, *Environ. Sci. Technol.*, *28*(9), 1615–1618.

Perry, K. D., S. S. Cliff, and M. P. Jimenez-Cruz (2004), Evidence for hygroscopic mineral dust particles from the Intercontinental Transport and Chemical Transformation Experiment, *J. Geophys. Res.*, *109*, D23S28, doi:10.1029/2004JD004979.

Prospero, J. M., P. Ginoux, O. Torres, S. E. Nicholson, and T. E. Gill (2002), Environmental characterization of global sources of atmospheric soil dust identified with the Nimbus 7 Total Ozone Mapping Spectrometer (TOMS) absorbing aerosol product, *Rev. Geophys.*, *40*(1), 1002, doi:10.1029/2000RG000095.

Pruppacher, H. R., and J. D. Klett (1997), *Microphysics of Clouds and Precipitation*, 2nd ed., Springer, New York.

Roberts, P., and J. Hallett (1968), A laboratory study of the ice nucleating properties of some mineral particulates, *Q. J. R. Meteorol. Soc.*, *94*, 25–34.

Rogers, D. C. (1988), Development of a continuous flow thermal gradient diffusion chamber for ice nucleation studies, *Atmos. Res.*, *22*, 149–181.

Rogers, D. C. (1994), Detecting ice nuclei with a continuous-flow diffusion chamber–Some exploratory tests of instrument response, *J. Atmos. Oceanic Technol.*, *11*, 1042–1047.

Rogers, D. C., P. J. DeMott, S. M. Kreidenweis, and Y. Chen (2001), A continuous-flow diffusion chamber for airborne measurements of ice nuclei, *J. Atmos. Oceanic Technol.*, *18*, 725–741, doi:10.1175/1520-0426.

Sassen, K. (2002), Indirect climate forcing from Asian dust storms, *Geophys. Res. Lett.*, *29*(10), 1465, doi:10.1029/2001GL014051.

Sassen, K. (2005), Dusty ice clouds over Alaska, *Nature*, *434*, 456, doi:10.1038/434456a.

Sassen, K., P. J. DeMott, J. M. Prospero, and M. R. Poellot (2003), Saharan dust storms and indirect aerosol effects on clouds: CRYSTAL-FACE results, *Geophys. Res. Lett.*, *30*(12), 1633, doi:10.1029/2003GL017371.

Seinfeld, J. H., and S. N. Pandis (1998), *Atmospheric Chemistry and Physics: From Air Pollution to Climate Change*, John Wiley, Hoboken, N. J.

Takemi, T. (2005), Explicit simulations of convective-scale transport of mineral dust in severe convective weather, *J. Meteorol. Soc. Jpn.*, *83A*, 187–203, doi:10.2151/jmsj.83A.187.

Thomson, D. S., M. E. Schein, and S. M. Murphy (2000), Particle analysis by Laser Mass Spectrometry Wb-57f Instrument overview, *Aerosol Sci. Technol.*, *33*, 153–169.

Twohy, C. H., and M. R. Poellot (2005), Chemical characteristics of ice residual nuclei in anvil cirrus clouds: Evidence for homogeneous and heterogeneous ice formation, *Atmos. Chem. Phys.*, *5*, 2289–2297.

VanCuren, R. A., and T. A. Cahill (2002), Asian aerosols in North America: Frequency and concentration of fine dust, *J. Geophys. Res.*, *107*(D24), 4804, doi:10.1029/2002JD002204.

van den Heever, S. C., and W. R. Cotton (2004), The impact of hail stone size on simulated supercell storms, *J. Atmos. Sci.*, *61*, 1596–1609, doi:10.1175/1520-0469(2004)061<1596:TIOHSO>2.0.CO;2.

Vassilev, S. V., G. M. Eskenazy, and C. G. Vassileva (2001), Behaviour of elements and minerals during preparation and combustion of the Pernik coal, Bulgaria, *Fuel. Process. Technol.*, *72*(2), 103–129.

Westphal, D. L., O. B. Toon, and T. N. Carlson (1988), A case-study of mobilization and transport of Saharan dust, *J. Atmos. Sci.*, *45*(15), 2145–2175.

Zhao, T. L., S. L. Gong, X. Y. Zhang, J. P. Blanchet, I. G. McKendry, and Z. J. Zhou (2006), A simulated climatology of Asian dust aerosol and its trans-Pacific transport. Part I: Mean climate and validation, *J. Clim.*, *19*(1), 88–103, doi:10.1175/JCLI3605.1.

Zuberi, B., A. K. Bertram, C. A. Cassa, L. T. Molina, and M. J. Molina (2002), Heterogeneous nucleation of ice in $(NH_4)_2SO_4$-H_2O particles with mineral dust immersions, *Geophys. Res. Lett.*, *29*(10), 1504, doi:10.1029/2001GL014289.

L. L. Ashbaugh, Crocker Nuclear Laboratory, University of California, Davis, CA 95616, USA.

R. D. Borys, Storm Peak Laboratory, Division of Atmospheric Science, Desert Research Institute, Reno, NV 89512, USA.

G. S. Casuccio and T. L. Lersch, RJ Lee Group, Inc., 350 Hochberg Road, Monroeville, PA 15146, USA.

D. J. Cziczo, Institute for Atmospheric and Climate Science, Swiss Federal Institute of Technology, CH-8092 Zurich, Switzerland.

P. J. DeMott, S. M. Kreidenweis, and M. S. Richardson, Department of Atmospheric Science, Colorado State University, Fort Collins, CO 80523, USA. (mattr@chem.atmos.colostate.edu)

E. J. Dunlea and J. L. Jimenez, Department of Chemistry and Biochemistry, Cooperative Institute for Research in Environmental Science, University of Colorado, Boulder, CO 80309, USA.

D. S. Thomson, Earth System Research Laboratory, NOAA, Boulder, CO 80305, USA.

D. L. Westphal, Naval Research Laboratory, Monterey, CA 93943, USA.